Title
Hydrogen Electrocatalysis on Perfluorosulfonic-Acid-Coated Pt

Journal
ACS Energy Letters, 11(4)

ISSN
2380-8195

Authors
Anderson, GraceC
Rajupet, Siddharth
Kushner, Douglas I
et al.

Publication Date
2026-04-10

DOI
10.1021/acsenergylett.6c00158

Hydrogen Electrocatalysis on PFSA-Coated Pt

Grace C. Anderson[‡ 1,2], Siddharth Rajupet[‡ 1,2], Douglas I. Kushner[2], Adam Z. Weber[2*], Clayton J. Radke[1*], Alexis T. Bell[1*]

[1]Department of Chemical and Biomolecular Engineering, University of California, Berkeley, California, USA, 94720

[2]Energy Technologies Area, Lawrence Berkeley National Laboratory, Berkeley, California, USA, 94720

For submission to

ACS Energy Letters

March 11, 2026

Corresponding authors: alexbell@berkley.edu; radke@berkeley.edu; azweber@lbl.gov

[‡] denotes equal contribution between G.C.A and S.R

ABSTRACT

Membrane-electrode assemblies utilize ionomer-coated electrocatalysts to achieve facile ion transport. Consequently, isolation of intrinsic catalyst kinetics from measured polarization curves is challenging, as properties of the catalyst and ionomer both affect the measurements. Here, we employ a Pt microelectrode coated by a thin perfluorosulfonic-acid (PFSA) layer to measure polarization curves for the HER/HOR. Intrinsic electrode kinetics are isolated by theoretical analysis of the local catalyst microenvironment accounting for mass-transport and thermodynamics. The observed enhancements in HER and HOR rates with increasing relative humidity (RH) at the working electrode are attributable to two competing factors: the decrease in activity of H^+ in the ionomer and the dominant decrease in the water reorganization energy in the Marcus–Hush–Chidsey representation of HER/HOR kinetics. The increase in intrinsic rate with increasing RH is attributed to increased H^+ transfer dynamics resulting from reduced confinement of water within the sub–nanometer water layer between the catalyst and ionomer as RH increases.

Membrane-electrode assemblies (MEAs) are electrochemical devices capable of operating at high current densities (~1 A/cm^2) and are therefore widely studied for applications including fuel cells, and water and CO_2 electrolyzers.[1–3] MEAs consist of two catalyst layers separated by an ionomer membrane that enables ion transport. In proton-exchange-membrane (PEM) fuel cells, the catalyst layers are complex porous networks of catalyst particles coated by inhomogeneous thin films of perfluorosulfonic-acid (PFSA) ionomer that provide ionic access to catalyst sites. Efficient ion transport requires hydration of both the PEM and ionomer within the catalyst layers by water supplied from humidified gas or liquid water.

The performance of MEAs, particularly PEM fuel cells, is strongly governed by the kinetics of each half reaction.[4] These kinetics are often represented using Butler-Volmer or Tafel kinetic models with effective rate parameters fit to MEA data.[5–7] Unfortunately, these approaches do not describe the intrinsic catalyst kinetics because the observed rates depend on properties of both the catalyst and the ionomer coating. Consequently, ionomer interactions with ions that dictate ion activity, and ion/molecular transport through the ionomer are convoluted with the intrinsic electrocatalysts kinetics. To determine the intrinsic kinetics of the catalyst requires an approach that clearly identifies the contribution of the ionomer coating to the observed polarization curves.

This work presents an experimental approach together with a theoretical framework that enables isolation of the intrinsic kinetic parameters for the hydrogen-oxidation and -evolution reactions (HOR and HER, respectively). HOR/HER are examined for their relevance to MEA-based fuel cells and electrolyzers and because their mechanisms are relatively straightforward.[8] Although measurement of the intrinsic kinetics for the HER/HOR is often encumbered by severe gas-transport limitations, this issue can be overcome by proper design of the experimental systems.[9–13]

We measure HER/HOR polarizations curves using a custom-built, three-electrode cell containing a 50-μm diameter polycrystalline Pt microelectrode surface coated by a ~40 nm thin layer of PFSA exposed to a gas with a defined relative humidity (RH), as shown in Figure 1.[14] Humidified 2% H_2 in Ar gas diffuses to/from the working microelectrode through a Pt-impregnated gas diffusion counter electrode (GDE) and the thin ionomer coating. Gas transport through the ionomer coating is rapid, enabling separation of the catalyst surface kinetics from gas-transport resistances.[9,10] Working and counter electrodes are ionically connected to a GDE reference electrode supplied with water-

saturated (100% RH) 2% H_2 in Ar gas. The entire cell is maintained at 30°C. Details of cell preparation and characterization are provided in Section S1 of the Supporting Information (SI).

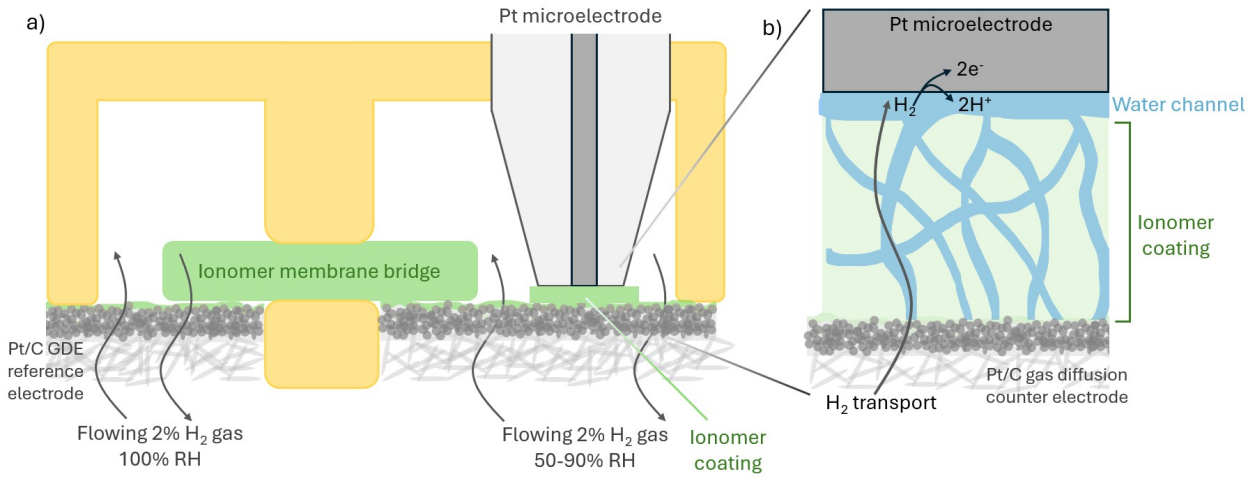

Figure 1. a) Microelectrode schematic with b) a zoomed-in representation of the interface of the Pt microelectrode, the humidified PFSA ionomer coating, and the Pt gas-diffusion-electrode counter electrode.

Figure S4 of the SI shows plots of the measured steady-state current density as a function of the total applied overpotential, η_{tot}, for 50, 70, and 90% RH gas supplied to the working electrode and averaged over three measurements. Negative overpotentials and current densities correspond to the HER, whereas positive values correspond to the HOR. The rates of both reactions increase with increasing RH. Figure S3 in the SI demonstrates that the electrochemically active surface area is invariant with RH, implying that humidity-dependent changes in HER/HOR rates reflect variations in intrinsic kinetic and ionomer properties rather than surface area. To decouple kinetic from ion-interaction, ohmic, and mass-transport effects in the ionomer, we developed a methodology and thermodynamic framework to calculate the H^+ activity in the ionomer and a gas-transport model to account for variation in H_2 concentration in the ionomer.

To interpret the polarization curves in Figure S4, we assume that the planar Pt microelectrode is separated from the ionomer coating by a thin, water-filled channel of thickness, D, as illustrated in 2. The channel thickness is governed by a balance between repulsive double layer forces and

attractive capillary forces, both of which depend on RH, along with the cell compression force (see Section S2 of the SI). This interfacial structure is supported by X-ray and neutron-scattering experiments indicating that contact between water-swollen ionomer and catalyst leads to formation of a nanoscale, water-filled channel at the electrocatalyst/ionomer interface.[15–17] PFSA retains its well-established phase-segregated structure and sulfonic-acid groups are effectively fully dissociated over the RH range studied.[18–20] Electrochemical reactions occur at the Stern plane, denoted by δ in the Figure 2.

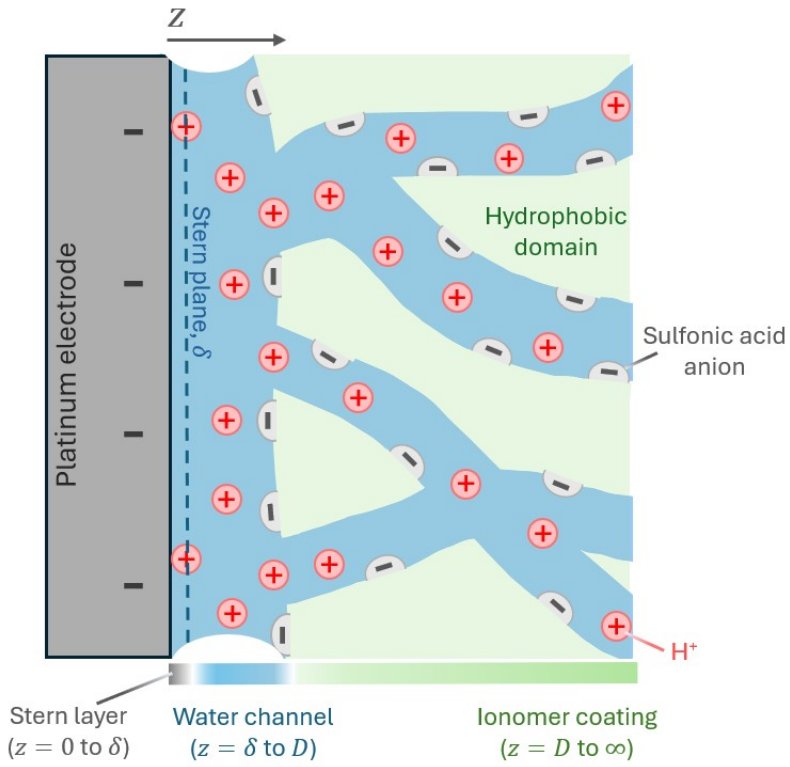

Figure 2. Schematic of the Pt/aqueous/ionomer interface regions. Potentials relevant for the HOR and HER are below the potential of zero charge of Pt (~0.3 V)[21] such that the surface is negatively charged. A 1-D representation of the interface is depicted below the schematic.

Acidic HER/HOR on Pt is thought to occur through a combination of Volmer ($H^{+}¿+e^{-}¿\leftrightarrow H_{ad}¿$), Tafel ($2\,H_{ad}\leftrightarrow H_2+2*¿$), or Heyrovsky ($H^{+}¿+H_{ad}+e^{-}¿\leftrightarrow H_2+¿¿$) steps. In aqueous solutions, the kinetics of these reactions are most often represented using Butler-Volmer formulations,[8,22–25] commonly assuming a Heyrovsky-Volmer[26,27] or a Volmer-Tafel mechanism.[28–30] However, more recent studies

show that HER/HOR in aqueous media depend strongly on the interfacial solvent structure, a factor that is not accounted for explicitly in Butler-Volmer kinetics,[22,31–40] but is well-captured by Marcus-Hush-Chidsey (MHC) theory through the solvent reorganization energy, λ_r.[38] Since RH likely influences water structure within the confined channel between the ionomer and the Pt surface, we apply MHC theory, after correcting for mass-transfer and ohmic losses, to describe the experimentally measured HER/HOR polarization curves.

The driving force for reaction in MHC theory is the activation overpotential, η_a, defined by

$$\eta_a = \eta_{tot} - \eta_\Omega - \eta_C \tag{1}$$

Here, the total overpotential, η_{tot}, is corrected by the ohmic resistive loss, η_Ω, and Nernstian shifts due to local gas concentrations, η_C. Section S3 of the SI describes the calculation of η_C and η_Ω based on limiting current and HFR measured from EIS, respectively. Figure 3a shows increased HFR and reduced limiting current at low RH as a consequence of hindered H^+ and H_2 transport through smaller ionomer aqueous domains at low RH.[18,41] Therefore, η_C and η_Ω corrections become larger as ionomer hydration decreases. Figure 4 presents experimental current density versus η_a, where the trend of faster HER/HOR rates with higher RH persists.

Following the work of Bazant and others,[42,43] the MHC formalism for the HER/HOR current density, i, is written as

$$i = A^{¿} a_{+,\delta} p_{H_2,\delta}^{\frac{1}{2}} \left(\frac{1}{p_{H_2,\delta}^{\frac{1}{2}} + a_{+,\delta} \exp\left(\tilde{\eta}_a\right)} - \frac{1}{a_{+,\delta} + p_{H_2,\delta}^{\frac{1}{2}} \exp\left(-\tilde{\eta}_a\right)} \right) erfc \left(\frac{\tilde{\lambda}_r - \sqrt{1 + \sqrt{\tilde{\lambda}_r} + \left(\tilde{\eta}_a + \ln\left(\frac{a}{p} \right. \right.}}{2\sqrt{\tilde{\lambda}_r}} \right.$$

(2)

where $\tilde{\eta}_a = \frac{F \eta_a}{RT}$ is the non-dimensional activation overpotential and $\tilde{\lambda}_r = \lambda_r / RT$ is the non-dimensional reorganization energy. The pre-exponential constant, $A^{¿}$, is defined in Section S3 of

the SI and depends primarily on the electronic coupling between the metal and redox species and the metal density of states. Subscript δ denotes quantities evaluated at the Stern plane. Equation 2 assumes that an electron-transfer step, during either the Volmer or Heyrovsky reaction steps, limits the rate of reaction which requires that λ_r is large relative to the ion-transfer free energies and η_a.[42] The significant experimental evidence that interfacial water affects HER/HOR kinetics[22,31–40] along with the strong energy of H^+ hydration[44] justifies this assumption.

Evaluation of Equation 2 requires the H_2 partial pressure, $p_{H_2,\delta}$, and the H^+ activity, $a_{+,\delta}$, at the Stern reaction plane. During HER, H_2 is produced at the Pt surface and, hence, $p_{H_2,\delta} > p_{H_2,\infty}$, whereas during HOR H_2 is consumed and $p_{H_2,\delta} < p_{H_2,\infty}$. We calculate $p_{H_2,\delta}$ by solving the 1-D steady-state diffusion of H_2 through the ionomer coating, as described in Section S3 of the SI. Mass-transfer limited H^+ transport through the ionomer is quantified from experimental limiting currents shown in Figure 3a.

The H^+ activity at the Stern plane, $a_{+,\delta}$, enters the reaction kinetics and may differ from that in the bulk ionomer coating if the electric potentials differ between these regions. However, calculations of the electric-potential distribution across the water channel and ionomer coating (Section S2) demonstrate that potentials at the Stern plane and in the ionomer are approximately equal. This results from the large concentration of H^+ that shields the negative charges on both Pt and ionomer, causing minimal electric potential variation beyond the Stern plane (Figure S6). Accordingly, $a_{+,\delta}$, is well-approximated by the bulk (electroneutral) ionomer H^+ activity, $a_{+¿¿}$ (*i.e.*, at ∞ in Figure 2) which varies with ionomer hydration (RH).

To evaluate $a_{+¿¿}$ we employ molecular-thermodynamics[45] to compute the excess chemical potentials for species in the bulk ionomer (Section S4 of the SI). H^+ molality (with water as the solvent) and the calculated excess chemical potential establish $a_{+¿¿}$ as a function of ionomer water uptake. Calculated activities are in excellent agreement with ion activities ascertained from a Gibb's-Duhem analysis of ionomer coatings (Figure S13) as well as experimental bulk aqueous acid activities at comparable concentrations (Figure S14). Notably, Figure S15 shows that H^+ ions are highly nonideal in the ionomer ($\gamma_{+¿□1¿}$). More importantly, Figure 3b shows that $a_{+¿¿}$ decreases with increasing RH as hydrophilic domains swell and the corresponding concentration of H^+

declines. This finding challenges prior assumptions that increasing humidity enhances kinetics by increasing H^+ activity.[46,47] The decrease of $a_{+¿¿}$ with increasing RH contradicts the trend of increasing HER/HOR rates with increasing RH in Figure 4. This contradiction is discussed below.

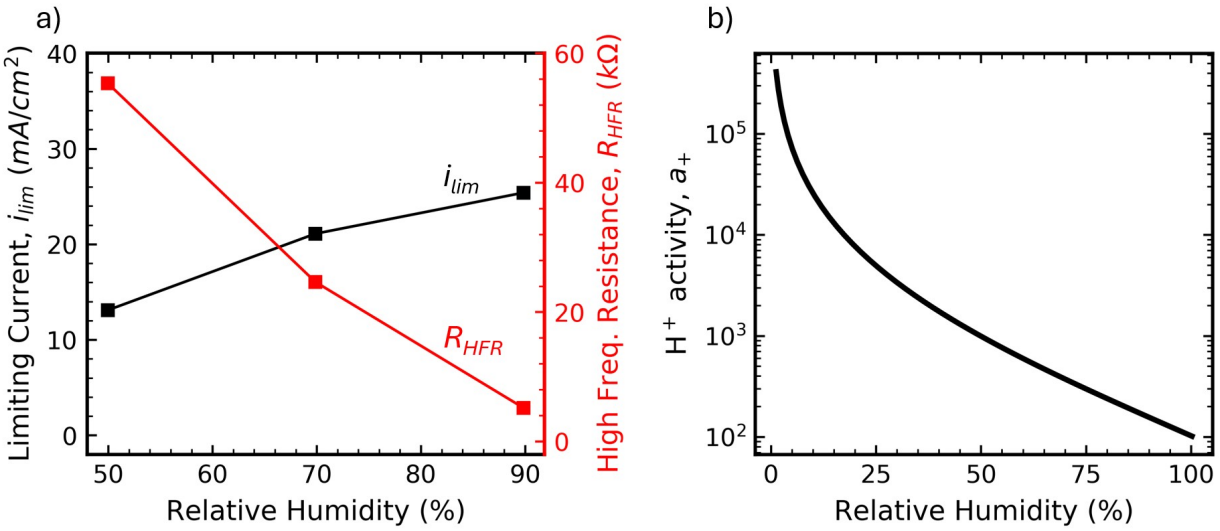

Figure 3. a) the experimentally measured limiting current (black) and high frequency resistance (red) as a function of RH. Lines are to guide the eye. b) H^+ activity calculated from molecular thermodynamics as a function of RH

To represent the data given in Figure 4 using MHC theory (Equation 2) requires evaluation of the parameters $A^{¿}$ and λ_r. The parameter $A^{¿}$, which represents the electronic coupling between Pt and H^+, is specific to Pt and is assumed to be independent of RH. Conversely, λ_r, the reorganization energy of water in the interfacial channel (Figure 2) may vary with RH if the channel thickness D changes. The value of $A^{¿}$was determined as described in Section S3 of the SI. Using $A^{¿}$= 197 A/cm^2 obtained from MHC fits to temperature-dependent MEA polarization curves measured by Durst *et al.*[10] (Figure S16), λ_r was adjusted for each RH to predict microelectrode polarization curves presented in Figure 4. These fits use the measured limiting current and calculated H^+ activity corresponding to each RH reported in Figure 3a and Table 1, respectively.

Solid curves in Figure 4 show the best fit of Equation 2 to the data, and the corresponding values of λ_r are summarized in Table 1. For RH = 90%, λ_r for the microelectrode (0.99 eV) is slightly larger than that from MEA measurements at RH = 100% (0.93 eV), consistent with the trend in RH in

Figure 4. This agreement indicates that kinetic parameters extracted from MEA studies are transferable to microelectrode experiments, despite the differences in catalyst form (Pt nanoparticles versus a polycrystalline Pt surface respectively), and validates the scaling of current density with H_2 partial pressure and temperature (Equation 2) that differed substantially between the microelectrode and MEA measurements. Overall, the agreement in A° and λ_r between this work and prior MEA studies demonstrates that intrinsic kinetic parameters can be reliably extracted from measured polarization curves, provided appropriate thermodynamic, ohmic, and mass-transport corrections are applied.

The value of λ_r for water in the Pt-ionomer gap of the microelectrode increases from 0.99 to 1.29 eV as RH decreases from 90 to 50%, corresponding to i_0 decreasing from 13.6 to 1.5 mA/cm^2 (Table 1). Lower i_0 values measured in the microelectrode cell relative to the MEA[10] arise from the lower concentration of H_2 used in the former experiments (2% versus 100%).

As shown in Figure 3b, H^+ ion activity in the ionomer coating and, hence, in the interfacial water layer, increases with decreasing RH, increasing the reaction rate. In contrast, Table 1 shows that λ_r also increases with decreasing RH indicating slower intrinsic kinetics. The latter trend suggests that water rearrangement required for electron transfer to H^+ becomes less facile at low RH. This trend can be rationalized by increased confinement of water within the interfacial channel of thickness *D*. The value of *D* is determined by a balance between the repulsive electric double-layer and the attractive capillary forces, with the latter increasing as RH decreases. As detailed in Section S2.2 of the SI, this force balance leads to a reduction of *D* from 0.8 to 0.4 nm as RH decreases from 90 to 50% (Figure S9), consistent with the neutron-reflectometry-measured length scales of water channels at PFSA-substrate interfaces.[15–17] Given the molecular size of water (0.28 nm), only a few water molecules occupy this channel. Experiments (including in PFSA membranes) and MD simulations show that such nanoconfined water is less mobile and highly structured, increasing resistance to water reorganization.[38,39,48–53] The effect is most pronounced at low RH, where stronger confinement reduces water mobility, consistent with prior studies showing that freely rotating water facilitates H^+ transfer and HER/HOR kinetics whereas increased rigidity suppresses reaction rates.[33,36–39,54,55]

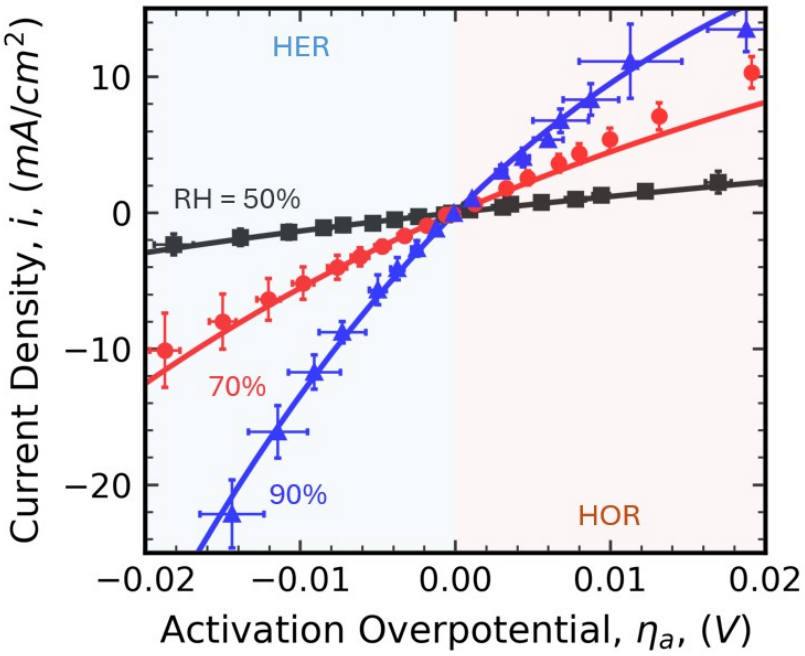

Figure 4. Current density versus activation overpotential for three different RH of the working electrode chamber: 50% RH (black), 70% RH (red), and 90% RH (blue). Points represent the experimental data, error bars represent a standard deviation, and the lines are the MHC kinetic fits using Equation 2, where 197 A cm^{-2} was used as the pre-factor A*. The overpotential, η_a, was calculated at each current density according to Eq. 1 (see Section S3 of the SI for details).

Table 1: Physical parameters as a function of RH.

RH	$a_{+¿¿}$	D	λ_r	i_0
Relative humidity	**H⁺ activity**	**Water-gap thickness [nm]**	**Reorganization energy [eV]**	**Exchange current density [mA cm^{-2}]**
50%	916	0.42	1.29	1.5
70%	352	0.52	1.11	6.0
90%	160	0.83	0.99	13.6

Figure 5 compares HER/HOR exchange current densities, i_0, for ionomer-coated Pt with those in aqueous acid solutions as a function of $a_{+¿¿}$. We note that in Figure 5 larger values of $a_{+¿¿}$ correspond to lower values of $-\log_{10}(a_{+¿})¿$ and pH. In aqueous electrolytes, i_0 increases with increasing $a_{+¿¿}$, reflecting both the explicit dependence of i_0 on $a_{+¿¿}$ in Equation S3.12, and a

reduced interfacial water reorganization energy at lower pH due to weaker electric fields across the Stern layer.[32,40,56,57] The weaker electric fields arise from smaller differences between the equilibrium potential and the potential of zero charge at low pH.[32,40,58–60]

To assess the dominant contribution to i_0, we predict i_0 versus $a_{+¿¿}$ in Figure 5 (gray-dashed line) using Equation S3.12 with $A^{¿}=197$ A/cm^2 and λ_r adjusted to a constant value of 0.7 eV. At higher $a_{+¿¿}$ ($a_{+¿>\ 10^{-3}¿}$), the model accurately captures the dependence of i_0 on $a_{+¿¿}$, indicating that changes in $a_{+¿¿}$ primarily govern i_0, whereas variations in λ_r are less important. This result highlights the critical role of the explicit dependence of i_0 on $a_{+¿¿}$, which is often overlooked in favor of indirect dependences through λ_r or H-binding energy.[32,40,52,61–66] At lower values of $a_{+¿¿}$, deviations from Equation S3.12 may arise from alkaline HER/HOR pathways[67] or changes in λ_r resulting from buffer cations introduced into the electrolyte to control the pH.[38] Figure S12 depicts i_0 versus $a_{+¿¿}$ using Equation S3.12 for varying values of λ_r.

In contrast to the dependence of i_0 on $a_{+¿¿}$ for aqueous acids, i_0 for ionomer-coated Pt decreases with increasing $a_{+¿¿}$ (decreasing RH). This behavior reflects two competing effects: increasing $a_{+¿¿}$ enhances i_0 according to Equation S3.12, whereas increased water confinement at lower RH impedes water reorganization and electron transfer. Confinement effects dominate causing i_0 to decrease as $a_{+¿¿}$ increases (and RH decreases), deviating from the trend predicted from Equation S3.12 with fixed λ_r. As RH approaches 100%, and the nanochannel thickens, confinement effects diminish and values of i_0 for aqueous and ionomer-coated Pt coincide (near $a_{+¿¿}$ = 100 in Figure 5). These results demonstrate that electrode kinetics in MEAs can differ substantially from those in aqueous acid solution due to nanoconfinement and water structuring. Accordingly, kinetic parameters used in MEA simulations should be derived from experiments that replicate catalyst-layer environments in MEAs.

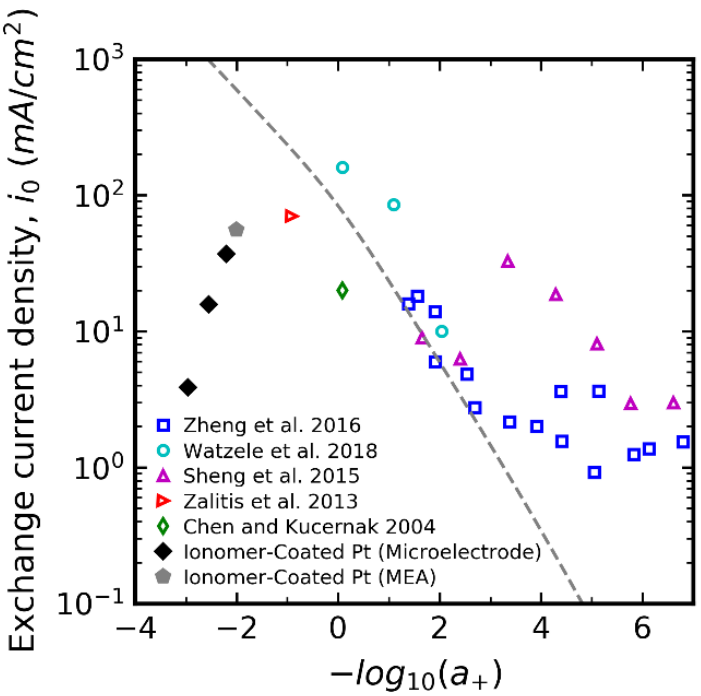

Figure 5. Exchange current density as a function of H^+ activity for HER/HOR in aqueous acid electrolyte[9,61,66,68,69] (open points) and in ionomer-coated Pt (filled points) measured in the present work and in Durst *et al.*[10] The values of i_0 for ionomer-coated Pt are taken from the microelectrode data in Figure 4 and MEA data reported by Durst *et al* (Figure S16).[13] These values of i_0 are adjusted to a common reference state of 100 kPa H_2 and 25°C using Equation S3.12. Specifically, $A^{¿}$=197 A/cm^2 is used throughout, with $a_{+¿¿}$ and λ_r taken from Table 1 for microelectrode data, and λ_r=0.93 eV and $a_{+¿=101.5¿}$ for the MEA data. The dashed gray line is predicted from MHC theory in Equation S3.12 where $A^{¿}$=197A/cm^2 and λ_r is adjusted to 0.7 eV to fit the data for aqueous acid solutions.

Improving electrochemical kinetics on ionomer-coated electrocatalyst requires minimizing λ_r while maintaining large $a_{+¿¿}$. This may be accomplished by tailoring the catalyst-ionomer interface to tune the interfacial water-channel thickness. Several factors influence the amount and structure of water at the Pt/ionomer interface, including ionomer equivalent weight and chemistry, coating thickness, annealing conditions, operating temperature, and catalyst structure. In general, lower equivalent weight, thicker ionomer coatings, and lower annealing temperatures promote greater water uptake at a given RH, whereas the effects of operating temperature and substrate are less straightforward.[18,68–75] Consequently, water reorganization is expected to be more facile under

conditions of higher water uptake, leading to faster kinetics. Further, enhancing repulsive interactions of the catalyst with the ionomer by tuning the catalyst PZC (*e.g.* through alloying strategies[32]) may also increase the thickness of the interfacial water-channel and improve kinetics. Testing these hypotheses is recommended in future studies of ionomer-coated catalysts. In addition, more direct measurements of the interfacial water layer thickness versus RH using neutron reflectometry are recommended,[15–17] along with IR characterization of the interfacial hydrogen water bond energies.[38]

Our study establishes a systematic methodology to correct for mass and ion transport as well as thermodynamic conditions to ensure measurement of intrinsic kinetics. The resulting kinetic analysis demonstrates that HER/HOR kinetic parameters for PFSA-coated Pt depend on both catalyst properties (A^{i}) and the properties of nanoconfined water separating the catalyst from the ionomer coating (λ_r). The ability of our theoretical framework to describe HER/HOR kinetics in both MEAs and microelectrode experiments demonstrates the generality of the approach and supports the intrinsic nature of the extracted kinetic parameters. Our results elucidate the commonly observed discrepancy between electrode kinetics in MEAs and in aqueous measurements[10,78,79] and emphasize the need to characterize kinetics under conditions that replicate the catalyst-layer microenvironment. Additional research is necessary to extend the approach reported here to other ionomer compositions and catalysts, as well as to the oxygen-evolution and -reduction reactions (OER and ORR), respectively.

ACKNOWLEDGEMENTS

The authors thank Dr. John G. Petrovick for his assistance with microelectrode training and for insightful discussions regarding mass transport calculations. This work was funded by the Hydrogen and Fuel Cell Technologies Program in the Critical Materials and Energy Innovation Office, of the U. S. Department of Energy under contract number DE-AC02-05CH11231, technology managers G. Kleen and D. Papageorgopoulos.

ASSOCIATED CONTENT

Description of experimental details and characterization (Section S1), evaluation of the electric-double layer extending from the Pt electrode surface and its impact on the nanochannel thickness and HER/HOR kinetics (Section S2), background regarding MHC kinetics and a gas transport model for evaluation of local H_2 concentrations (Section S3), thermodynamic model for the H^+ activity and its validation (Section S4), and application of theoretical analysis to extract intrinsic kinetic parameters from MEA data from Durst *et al.*[10](Section S5)

AUTHOR INFORMATION

Corresponding Authors

Alexis T. Bell — *Department of Chemical and Biomolecular Engineering, University of California, Berkeley, California, 94720, United States;*

Email: alexbell@berkeley.edu

Clayton J. Radke — *Department of Chemical and Biomolecular Engineering, University of California, Berkeley, California, 94720, United States;*

Email: radke@berkeley.edu

Adam Z. Weber — *Energy Technologies Area, Lawrence Berkeley National Laboratory, Berkeley, California, 94720, United States;*

Email: azweber@lbl.gov

Authors

Grace C. Anderson — *Department of Chemical and Biomolecular Engineering, University of California, Berkeley, California, 94720, United States;*

Siddharth Rajupet — *Department of Chemical and Biomolecular Engineering, University of California, Berkeley, California, 94720, United States;*

Douglas I. Kushner — *Energy Technologies Area, Lawrence Berkeley National Laboratory, Berkeley, California, 94720, United States;*

REFERNCES

(1) Wang, Y.; Chen, K. S.; Mishler, J.; Cho, S. C.; Adroher, X. C. A Review of Polymer Electrolyte Membrane Fuel Cells: Technology, Applications, and Needs on Fundamental Research. *Applied Energy* **2011**, *88* (4), 981–1007. https://doi.org/10.1016/j.apenergy.2010.09.030.

(2) Zhang, Z.; Huang, X.; Chen, Z.; Zhu, J.; Endrődi, B.; Janáky, C.; Deng, D. Membrane Electrode Assembly for Electrocatalytic CO2 Reduction: Principle and Application. *Angewandte Chemie* **2023**, *135* (28), e202302789. https://doi.org/10.1002/ange.202302789.

(3) Millet, P.; Ngameni, R.; Grigoriev, S. A.; Mbemba, N.; Brisset, F.; Ranjbari, A.; Etiévant, C. PEM Water Electrolyzers: From Electrocatalysis to Stack Development. *International Journal of Hydrogen Energy* **2010**, *35* (10), 5043–5052. https://doi.org/10.1016/j.ijhydene.2009.09.015.

(4) Xiao, F.; Wang, Y.-C.; Wu, Z.-P.; Chen, G.; Yang, F.; Zhu, S.; Siddharth, K.; Kong, Z.; Lu, A.; Li, J.-C.; Zhong, C.-J.; Zhou, Z.-Y.; Shao, M. Recent Advances in Electrocatalysts for Proton Exchange Membrane Fuel Cells and Alkaline Membrane Fuel Cells. *Advanced Materials* **2021**, *33* (50), 2006292. https://doi.org/10.1002/adma.202006292.

(5) Dickinson, E. J. F.; Hinds, G. The Butler-Volmer Equation for Polymer Electrolyte Membrane Fuel Cell (PEMFC) Electrode Kinetics: A Critical Discussion. *J. Electrochem. Soc.* **2019**, *166* (4), F221. https://doi.org/10.1149/2.0361904jes.

(6) Zenyuk, I. V.; Das, P. K.; Weber, A. Z. Understanding Impacts of Catalyst-Layer Thickness on Fuel-Cell Performance via Mathematical Modeling. *J. Electrochem. Soc.* **2016**, *163* (7), F691. https://doi.org/10.1149/2.1161607jes.

(7) Weber, A. Z.; Borup, R. L.; Darling, R. M.; Das, P. K.; Dursch, T. J.; Gu, W.; Harvey, D.; Kusoglu, A.; Litster, S.; Mench, M. M.; Mukundan, R.; Owejan, J. P.; Pharoah, J. G.; Secanell, M.; Zenyuk, I. V. A Critical Review of Modeling Transport Phenomena in Polymer-Electrolyte Fuel Cells. *J. Electrochem. Soc.* **2014**, *161* (12), F1254–F1299. https://doi.org/10.1149/2.0751412jes.

(8) Kucernak, A. R.; Zalitis, C. General Models for the Electrochemical Hydrogen Oxidation and Hydrogen Evolution Reactions: Theoretical Derivation and Experimental Results under Near Mass-Transport Free Conditions. *J. Phys. Chem. C* **2016**, *120* (20), 10721–10745. https://doi.org/10.1021/acs.jpcc.6b00011.

(9) Chen, S.; Kucernak, A. Electrocatalysis under Conditions of High Mass Transport: Investigation of Hydrogen Oxidation on Single Submicron Pt Particles Supported on Carbon. *J. Phys. Chem. B* **2004**, *108* (37), 13984–13994. https://doi.org/10.1021/jp048641u.

(10) Durst, J.; Simon, C.; Hasché, F.; Gasteiger, H. A. Hydrogen Oxidation and Evolution Reaction Kinetics on Carbon Supported Pt, Ir, Rh, and Pd Electrocatalysts in Acidic Media. *J. Electrochem. Soc.* **2014**, *162* (1), F190. https://doi.org/10.1149/2.0981501jes.
(11) Zalitis, C. M.; Sharman, J.; Wright, E.; Kucernak, A. R. Properties of the Hydrogen Oxidation Reaction on Pt/C Catalysts at Optimised High Mass Transport Conditions and Its Relevance to the Anode Reaction in PEFCs and Cathode Reactions in Electrolysers. *Electrochimica Acta* **2015**, *176*, 763–776. https://doi.org/10.1016/j.electacta.2015.06.146.
(12) Schmitt, N.; Schmidt, M.; Mueller, J. E.; Schmidt, L.; Trabold, M.; Jeschonek, K.; Etzold, B. J. M. Which Insights Can Gas Diffusion Electrode Half-Cell Experiments Give into Activity Trends and Transport Phenomena of Membrane Electrode Assemblies? *Energy Adv.* **2023**, *2* (6), 854–863. https://doi.org/10.1039/D3YA00055A.
(13) Ehelebe, K.; Seeberger, D.; Paul, M. T. Y.; Thiele, S.; Mayrhofer, K. J. J.; Cherevko, S. Evaluating Electrocatalysts at Relevant Currents in a Half-Cell: The Impact of Pt Loading on Oxygen Reduction Reaction. *J. Electrochem. Soc.* **2019**, *166* (16), F1259. https://doi.org/10.1149/2.0911915jes.
(14) Petrovick, J. G.; Anderson, G. C.; Kushner, D. I.; Danilovic, N.; Weber, A. Z. Method—Using Microelectrodes to Explore Solid Polymer Electrolytes. *J. Electrochem. Soc.* **2021**, *168* (5), 056517. https://doi.org/10.1149/1945-7111/abee5f.
(15) DeCaluwe, S. C.; Kienzle, P. A.; Bhargava, P.; Baker, A. M.; Dura, J. A. Phase Segregation of Sulfonate Groups in Nafion Interface Lamellae, Quantified via Neutron Reflectometry Fitting Techniques for Multi-Layered Structures. *Soft Matter* **2014**, *10* (31), 5763–5776. https://doi.org/10.1039/C4SM00850B.
(16) Shrivastava, U. N.; Fritzsche, H.; Karan, K. Interfacial and Bulk Water in Ultrathin Films of Nafion, 3M PFSA, and 3M PFIA Ionomers on a Polycrystalline Platinum Surface. *Macromolecules* **2018**, *51* (23), 9839–9849. https://doi.org/10.1021/acs.macromol.8b01240.
(17) Dura, J. A.; Kim, S.; Page, K. A.; Soles, C. L. Controlling Polymer Electrolyte Interfacial Morphology through Chemical Interactions. *Chem. Mater.* **2025**, *37* (17), 6921–6931. https://doi.org/10.1021/acs.chemmater.5c01738.
(18) Kusoglu, A.; Weber, A. Z. New Insights into Perfluorinated Sulfonic-Acid Ionomers. *Chem. Rev.* **2017**, *117* (3), 987–1104. https://doi.org/10.1021/acs.chemrev.6b00159.
(19) Agarwal, T.; Prasad, A. K.; Advani, S. G.; Babu, S. K.; Borup, R. L. Infrared Spectroscopy for Understanding the Structure of Nafion and Its Associated Properties. *J. Mater. Chem. A* **2024**, *12* (24), 14229–14244. https://doi.org/10.1039/D3TA05653H.
(20) Grosmaire, L.; Castagnoni, S.; Huguet, P.; Sistat, P.; Boucher, M.; Bouchard, P.; Bébin, P.; Deabate, S. Probing Proton Dissociation in Ionic Polymers by Means of in Situ ATR-FTIR Spectroscopy. **2008**. https://doi.org/10.1039/B714870D.
(21) Rizo, R.; Sitta, E.; Herrero, E.; Climent, V.; Feliu, J. M. Towards the Understanding of the Interfacial pH Scale at Pt(1 1 1) Electrodes. *Electrochimica Acta* **2015**, *162*, 138–145. https://doi.org/10.1016/j.electacta.2015.01.069.
(22) Dubouis, N.; Grimaud, A. The Hydrogen Evolution Reaction: From Material to Interfacial Descriptors. *Chemical Science* **2019**, *10* (40), 9165–9181. https://doi.org/10.1039/C9SC03831K.

(23) Lasia, A. Mechanism and Kinetics of the Hydrogen Evolution Reaction. *International Journal of Hydrogen Energy* **2019**, *44* (36), 19484–19518. https://doi.org/10.1016/j.ijhydene.2019.05.183.
(24) Prats, H.; Chan, K. The Determination of the HOR/HER Reaction Mechanism from Experimental Kinetic Data. *Phys. Chem. Chem. Phys.* **2021**, *23* (48), 27150–27158. https://doi.org/10.1039/D1CP04134G.
(25) Skúlason, E.; Tripkovic, V.; Björketun, M. E.; Gudmundsdóttir, S.; Karlberg, G.; Rossmeisl, J.; Bligaard, T.; Jónsson, H.; Nørskov, J. K. Modeling the Electrochemical Hydrogen Oxidation and Evolution Reactions on the Basis of Density Functional Theory Calculations. *J. Phys. Chem. C* **2010**, *114* (42), 18182–18197. https://doi.org/10.1021/jp1048887.
(26) Gao, G.; Wang, L.-W. A Potential and pH Inclusive Microkinetic Model for Hydrogen Reactions on Pt Surface. *Chem Catalysis* **2021**, *1* (6), 1331–1345. https://doi.org/10.1016/j.checat.2021.10.006.
(27) Tavares, M. C.; Machado, S. A. S.; Mazo, L. H. Study of Hydrogen Evolution Reaction in Acid Medium on Pt Microelectrodes. *Electrochimica Acta* **2001**, *46* (28), 4359–4369. https://doi.org/10.1016/S0013-4686(01)00726-5.
(28) Stühmeier, B. M.; Pietsch, M. R.; Schwämmlein, J. N.; Gasteiger, H. A. Pressure and Temperature Dependence of the Hydrogen Oxidation and Evolution Reaction Kinetics on Pt Electrocatalysts via PEMFC-Based Hydrogen-Pump Measurements. *J. Electrochem. Soc.* **2021**, *168* (6), 064516. https://doi.org/10.1149/1945-7111/ac099c.
(29) Shinagawa, T.; Garcia-Esparza, A. T.; Takanabe, K. Insight on Tafel Slopes from a Microkinetic Analysis of Aqueous Electrocatalysis for Energy Conversion. *Sci Rep* **2015**, *5* (1), 13801. https://doi.org/10.1038/srep13801.
(30) Kucernak, A. R.; Zalitis, C. General Models for the Electrochemical Hydrogen Oxidation and Hydrogen Evolution Reactions: Theoretical Derivation and Experimental Results under Near Mass-Transport Free Conditions. *J. Phys. Chem. C* **2016**, *120* (20), 10721–10745. https://doi.org/10.1021/acs.jpcc.6b00011.
(31) Baidoun, R.; Liu, G.; Kim, D. Recent Advances in the Role of Interfacial Liquids in Electrochemical Reactions. *Nanoscale* **2024**, *16* (12), 5903–5925. https://doi.org/10.1039/D3NR06092F.
(32) Ledezma-Yanez, I.; Wallace, W. D. Z.; Sebastián-Pascual, P.; Climent, V.; Feliu, J. M.; Koper, M. T. M. Interfacial Water Reorganization as a pH-Dependent Descriptor of the Hydrogen Evolution Rate on Platinum Electrodes. *Nat Energy* **2017**, *2* (4), 1–7. https://doi.org/10.1038/nenergy.2017.31.
(33) Sarabia, F. J.; Sebastián-Pascual, P.; Koper, M. T. M.; Climent, V.; Feliu, J. M. Effect of the Interfacial Water Structure on the Hydrogen Evolution Reaction on Pt(111) Modified with Different Nickel Hydroxide Coverages in Alkaline Media. *ACS Appl. Mater. Interfaces* **2019**, *11* (1), 613–623. https://doi.org/10.1021/acsami.8b15003.
(34) Sun, Q.; Oliveira, N. J.; Kwon, S.; Tyukhtenko, S.; Guo, J. J.; Myrthil, N.; Lopez, S. A.; Kendrick, I.; Mukerjee, S.; Ma, L.; Ehrlich, S. N.; Li, J.; Goddard, W. A.; Yan, Y.; Jia, Q. Understanding Hydrogen Electrocatalysis by Probing the Hydrogen-Bond Network of Water at the Electrified Pt–Solution Interface. *Nat Energy* **2023**, *8* (8), 859–869. https://doi.org/10.1038/s41560-023-01302-y.

(35) Intikhab, S.; Rebollar, L.; Li, Y.; Pai, R.; Kalra, V.; Tang, M. H.; Snyder, J. D. Caffeinated Interfaces Enhance Alkaline Hydrogen Electrocatalysis. *ACS Catal.* **2020**, *10* (12), 6798–6802. https://doi.org/10.1021/acscatal.0c01635.

(36) Chai, J.; Zheng, Z.; Pan, H.; Zhang, S.; Lakshmi, K. V.; Sun, Y.-Y. Significance of Hydrogen Bonding Networks in the Proton-Coupled Electron Transfer Reactions of Photosystem II from a Quantum-Mechanics Perspective. *Phys. Chem. Chem. Phys.* **2019**, *21* (17), 8721–8728. https://doi.org/10.1039/C9CP00868C.

(37) Rollins, J. B.; Conboy, J. C. Kinetics and Thermodynamics of Hydrogen Oxidation and Oxygen Reduction in Hydrophobic Room-Temperature Ionic Liquids. *J Electrochem Soc* **2009**, *156* (8), B943–B954. https://doi.org/10.1149/1.3143122.

(38) Huang, B.; Rao, R. R.; You, S.; Hpone Myint, K.; Song, Y.; Wang, Y.; Ding, W.; Giordano, L.; Zhang, Y.; Wang, T.; Muy, S.; Katayama, Y.; Grossman, J. C.; Willard, A. P.; Xu, K.; Jiang, Y.; Shao-Horn, Y. Cation- and pH-Dependent Hydrogen Evolution and Oxidation Reaction Kinetics. *JACS Au* **2021**, *1* (10), 1674–1687. https://doi.org/10.1021/jacsau.1c00281.

(39) Wang, T.; Iriawan, H.; Peng, J.; Rao, R. R.; Huang, B.; Zheng, D.; Menga, D.; Aggarwal, A.; Yuan, S.; Eom, J.; Zhang, Y.; McCormack, K.; Román-Leshkov, Y.; Grossman, J.; Shao-Horn, Y. Confined Water for Catalysis: Thermodynamic Properties and Reaction Kinetics. *Chem. Rev.* **2025**, *125* (3), 1420–1467. https://doi.org/10.1021/acs.chemrev.4c00274.

(40) Sebastián-Pascual, P.; Herzog, A.; Zhang, Y.; Shao-Horn, Y.; Escudero-Escribano, M. Electrolyte Effects in Proton–Electron Transfer Reactions and Implications for Renewable Fuels and Chemicals Synthesis. *Nat Catal* **2025**, *8* (10), 986–999. https://doi.org/10.1038/s41929-025-01421-7.

(41) Petrovick, J. G.; Radke, C. J.; Weber, A. Z. Gas Mass-Transport Coefficients in Ionomer Membranes Using a Microelectrode. *ACS Meas. Sci. Au* **2022**, *2* (3), 208–218. https://doi.org/10.1021/acsmeasuresciau.1c00058.

(42) Bazant, M. Z. Unified Quantum Theory of Electrochemical Kinetics by Coupled Ion–Electron Transfer. *Faraday Discuss.* **2023**, *246* (0), 60–124. https://doi.org/10.1039/D3FD00108C.

(43) Zeng, Y.; Smith, R. B.; Bai, P.; Bazant, M. Z. Simple Formula for Marcus–Hush–Chidsey Kinetics. *Journal of Electroanalytical Chemistry* **2014**, *735*, 77–83. https://doi.org/10.1016/j.jelechem.2014.09.038.

(44) Santos, E.; Lundin, A.; Pötting, K.; Quaino, P.; Schmickler, W. Model for the Electrocatalysis of Hydrogen Evolution. *Phys. Rev. B* **2009**, *79* (23), 235436. https://doi.org/10.1103/PhysRevB.79.235436.

(45) Crothers, A. R.; Darling, R. M.; Kusoglu, A.; Radke, C. J.; Weber, A. Z. Theory of Multicomponent Phenomena in Cation-Exchange Membranes: Part I. Thermodynamic Model and Validation. *J. Electrochem. Soc.* **2020**, *167* (1), 013547. https://doi.org/10.1149/1945-7111/ab6723.

(46) Neyerlin, K. C.; Gu, W.; Jorne, J.; Gasteiger, H. A. Study of the Exchange Current Density for the Hydrogen Oxidation and Evolution Reactions. *J. Electrochem. Soc.* **2007**, *154* (7), B631. https://doi.org/10.1149/1.2733987.

(47) Xu, H.; Song, Y.; Kunz, H. R.; Fenton, J. M. Effect of Elevated Temperature and Reduced Relative Humidity on ORR Kinetics for PEM Fuel Cells. *J. Electrochem. Soc.* **2005**, *152* (9), A1828. https://doi.org/10.1149/1.1984351.

(48) Spry, D. B.; Goun, A.; Glusac, K.; Moilanen, D. E.; Fayer, M. D. Proton Transport and the Water Environment in Nafion Fuel Cell Membranes and AOT Reverse Micelles. *J. Am. Chem. Soc.* **2007**, *129* (26), 8122–8130. https://doi.org/10.1021/ja071939o.
(49) Gonella, G.; Backus, E. H. G.; Nagata, Y.; Bonthuis, D. J.; Loche, P.; Schlaich, A.; Netz, R. R.; Kühnle, A.; McCrum, I. T.; Koper, M. T. M.; Wolf, M.; Winter, B.; Meijer, G.; Campen, R. K.; Bonn, M. Water at Charged Interfaces. *Nat Rev Chem* **2021**, *5* (7), 466–485. https://doi.org/10.1038/s41570-021-00293-2.
(50) Shi, G.; Lu, T.; Zhang, L. Understanding the Interfacial Water Structure in Electrocatalysis. *Natl Sci Rev* **2024**, *11* (12), nwae241. https://doi.org/10.1093/nsr/nwae241.
(51) Bangle, R. E.; Schneider, J.; Conroy, D. T.; Aramburu-Trošelj, B. M.; Meyer, G. J. Kinetic Evidence That the Solvent Barrier for Electron Transfer Is Absent in the Electric Double Layer. *J. Am. Chem. Soc.* **2020**, *142* (35), 14940–14946. https://doi.org/10.1021/jacs.0c05226.
(52) Huang, B.; Myint, K. H.; Wang, Y.; Zhang, Y.; Rao, R. R.; Sun, J.; Muy, S.; Katayama, Y.; Corchado Garcia, J.; Fraggedakis, D.; Grossman, J. C.; Bazant, M. Z.; Xu, K.; Willard, A. P.; Shao-Horn, Y. Cation-Dependent Interfacial Structures and Kinetics for Outer-Sphere Electron-Transfer Reactions. *J. Phys. Chem. C* **2021**, *125* (8), 4397–4411. https://doi.org/10.1021/acs.jpcc.0c10492.
(53) Fumagalli, L.; Esfandiar, A.; Fabregas, R.; Hu, S.; Ares, P.; Janardanan, A.; Yang, Q.; Radha, B.; Taniguchi, T.; Watanabe, K.; Gomila, G.; Novoselov, K. S.; Geim, A. K. Anomalously Low Dielectric Constant of Confined Water. *Science* **2018**, *360* (6395), 1339–1342. https://doi.org/10.1126/science.aat4191.
(54) Intikhab, S.; Rebollar, L.; Li, Y.; Pai, R.; Kalra, V.; Tang, M. H.; Snyder, J. D. Caffeinated Interfaces Enhance Alkaline Hydrogen Electrocatalysis. *ACS Catal.* **2020**, *10* (12), 6798–6802. https://doi.org/10.1021/acscatal.0c01635.
(55) Shibata, M. S.; Morimoto, Y.; Zenyuk, I. V.; Weber, A. Z. Parameter-Fitting-Free Continuum Modeling of Electric Double Layer in Aqueous Electrolyte. *J. Chem. Theory Comput.* **2024**. https://doi.org/10.1021/acs.jctc.4c00408.
(56) Darlington, A. M.; Jarisz, T. A.; DeWalt-Kerian, E. L.; Roy, S.; Kim, S.; Azam, Md. S.; Hore, D. K.; Gibbs, J. M. Separating the pH-Dependent Behavior of Water in the Stern and Diffuse Layers with Varying Salt Concentration. *J. Phys. Chem. C* **2017**, *121* (37), 20229–20241. https://doi.org/10.1021/acs.jpcc.7b03522.
(57) Ojha, K.; Doblhoff-Dier, K.; Koper, M. T. M. Double-Layer Structure of the Pt(111)–Aqueous Electrolyte Interface. *Proceedings of the National Academy of Sciences* **2022**, *119* (3), e2116016119. https://doi.org/10.1073/pnas.2116016119.
(58) Waegele, M. M.; Gunathunge, C. M.; Li, J.; Li, X. How Cations Affect the Electric Double Layer and the Rates and Selectivity of Electrocatalytic Processes. *J. Chem. Phys.* **2019**, *151* (16), 160902. https://doi.org/10.1063/1.5124878.
(59) Cui, W.-G.; Gao, F.; Na, G.; Wang, X.; Li, Z.; Yang, Y.; Niu, Z.; Qu, Y.; Wang, D.; Pan, H. Insights into the pH Effect on Hydrogen Electrocatalysis. *Chem. Soc. Rev.* **2024**, *53* (20), 10253–10311. https://doi.org/10.1039/D4CS00370E.
(60) Groß, A. Reversible vs Standard Hydrogen Electrode Scale in Interfacial Electrochemistry from a Theoretician's Atomistic Point of View. *J. Phys. Chem. C* **2022**, *126* (28), 11439–11446. https://doi.org/10.1021/acs.jpcc.2c02734.

(61) Sheng, W.; Zhuang, Z.; Gao, M.; Zheng, J.; Chen, J. G.; Yan, Y. Correlating Hydrogen Oxidation and Evolution Activity on Platinum at Different pH with Measured Hydrogen Binding Energy. *Nat Commun* **2015**, *6* (1), 5848. https://doi.org/10.1038/ncomms6848.
(62) Durst, J.; Siebel, A.; Simon, C.; Hasché, F.; Herranz, J.; Gasteiger, H. A. New Insights into the Electrochemical Hydrogen Oxidation and Evolution Reaction Mechanism. *Energy Environ. Sci.* **2014**, *7* (7), 2255–2260. https://doi.org/10.1039/C4EE00440J.
(63) Cheng, T.; Wang, L.; Merinov, B. V.; Goddard, W. A. I. Explanation of Dramatic pH-Dependence of Hydrogen Binding on Noble Metal Electrode: Greatly Weakened Water Adsorption at High pH. *J. Am. Chem. Soc.* **2018**, *140* (25), 7787–7790. https://doi.org/10.1021/jacs.8b04006.
(64) Mitchell, J. B.; Shen, M.; Twight, L.; Boettcher, S. W. Hydrogen-Evolution-Reaction Kinetics pH Dependence: Is It Covered? *Chem Catalysis* **2022**, *2* (2), 236–238. https://doi.org/10.1016/j.checat.2022.02.001.
(65) Nørskov, J. K.; Bligaard, T.; Logadottir, A.; Kitchin, J. R.; Chen, J. G.; Pandelov, S.; Stimming, U. Trends in the Exchange Current for Hydrogen Evolution. *J. Electrochem. Soc.* **2005**, *152* (3), J23. https://doi.org/10.1149/1.1856988.
(66) Zheng, J.; Sheng, W.; Zhuang, Z.; Xu, B.; Yan, Y. Universal Dependence of Hydrogen Oxidation and Evolution Reaction Activity of Platinum-Group Metals on pH and Hydrogen Binding Energy. *Science Advances* **2016**, *2* (3), e1501602. https://doi.org/10.1126/sciadv.1501602.
(67) Zhou, Z.; Pei, Z.; Wei, L.; Zhao, S.; Jian, X.; Chen, Y. Electrocatalytic Hydrogen Evolution under Neutral pH Conditions: Current Understandings, Recent Advances, and Future Prospects. *Energy Environ. Sci.* **2020**, *13* (10), 3185–3206. https://doi.org/10.1039/D0EE01856B.
(68) Watzele, S.; Fichtner, J.; Garlyyev, B.; Schwämmlein, J. N.; Bandarenka, A. S. On the Dominating Mechanism of the Hydrogen Evolution Reaction at Polycrystalline Pt Electrodes in Acidic Media. *ACS Catalysis* **2018**, *8* (10), 9456–9462. https://doi.org/10.1021/acscatal.8b03365.
(69) M. Zalitis, C.; Kramer, D.; R. Kucernak, A. Electrocatalytic Performance of Fuel Cell Reactions at Low Catalyst Loading and High Mass Transport. **2013**. https://doi.org/10.1039/C3CP44431G.
(70) Poojary, S.; Islam, M. N.; Shrivastava, U. N.; Roberts, E. P. L.; Karan, K. Transport and Electrochemical Interface Properties of Ionomers in Low-Pt Loading Catalyst Layers: Effect of Ionomer Equivalent Weight and Relative Humidity. *Molecules* **2020**, *25* (15), 3387. https://doi.org/10.3390/molecules25153387.
(71) DeCaluwe, S. C.; Dura, J. A. Finite Thickness Effects on Nafion Water Uptake and Ionic Conductivity at Hydrophilic Substrate Interfaces, and Implications for PEMFC Performance. *ECS Trans.* **2017**, *80* (8), 619. https://doi.org/10.1149/08008.0619ecst.
(72) Eskandari, H.; Paul, D. K.; Young, A. P.; Karan, K. Humidity-Dependent Hydration and Proton Conductivity of PFSA Ionomer Thin Films at Fuel-Cell-Relevant Temperatures: Effect of Ionomer Equivalent Weight and Side-Chain Characteristics. *ACS Appl. Mater. Interfaces* **2022**, *14* (45), 50762–50772. https://doi.org/10.1021/acsami.2c12667.

(73) Hensley, J. E.; Way, J. D.; Dec, S. F.; Abney, K. D. The Effects of Thermal Annealing on Commercial Nafion® Membranes. *Journal of Membrane Science* **2007**, *298* (1), 190–201. https://doi.org/10.1016/j.memsci.2007.04.019.
(74) Lyulin, A. V.; Sengupta, S.; Varughese, A.; Komarov, P.; Venkatnathan, A. Effect of Annealing on Structure and Diffusion in Hydrated Nafion Membranes. *ACS Appl. Polym. Mater.* **2020**, *2* (11), 5058–5066. https://doi.org/10.1021/acsapm.0c00875.
(75) Ono, Y.; Nagao, Y. Interfacial Structure and Proton Conductivity of Nafion at the Pt-Deposited Surface. *Langmuir* **2016**, *32* (1), 352–358. https://doi.org/10.1021/acs.langmuir.5b02623.
(76) Duan, Q.; Wang, H.; Benziger, J. Transport of Liquid Water through Nafion Membranes. *Journal of Membrane Science* **2012**, *392–393*, 88–94. https://doi.org/10.1016/j.memsci.2011.12.004.
(77) Murthi, V. S.; Dura, J.; Satija, S.; Majkrzak, C. Water Uptake and Interfacial Structural Changes of Thin Film Nafion® Membranes Measured by Neutron Reflectivity for PEM Fuel Cells. *ECS Trans.* **2008**, *16* (2), 1471. https://doi.org/10.1149/1.2981988.
(78) Fan, J.; Chen, M.; Zhao, Z.; Zhang, Z.; Ye, S.; Xu, S.; Wang, H.; Li, H. Bridging the Gap between Highly Active Oxygen Reduction Reaction Catalysts and Effective Catalyst Layers for Proton Exchange Membrane Fuel Cells. *Nat Energy* **2021**, *6* (5), 475–486. https://doi.org/10.1038/s41560-021-00824-7.
(79) Lazaridis, T.; Stühmeier, B. M.; Gasteiger, H. A.; El-Sayed, H. A. Capabilities and Limitations of Rotating Disk Electrodes versus Membrane Electrode Assemblies in the Investigation of Electrocatalysts. *Nat Catal* **2022**, *5* (5), 363–373. https://doi.org/10.1038/s41929-022-00776-5.

TOC Graphic